Atmospheric Environment 45 (2011) 2522–2530

Contents lists available at ScienceDirect

Atmospheric Environment

journal homepage: www.elsevier.com/locate/atmosenv

Model evaluation of roadside barrier impact on near-road air pollution

Gayle S.W. Hagler [a,*], Wei Tang [b], Matthew J. Freeman [b], David K. Heist [c], Steven G. Perry [c], Alan F. Vette [c]

[a] US EPA, Office of Research and Development, National Risk Management Research Laboratory, Research Triangle Park, NC 27711, USA
[b] Lockheed Martin Corporation, Information Systems & Global Services, Durham, NC, USA
[c] US EPA, Office of Research and Development, National Exposure Research Laboratory, Research Triangle Park, NC, USA

ARTICLE INFO

Article history:
Received 19 August 2010
Received in revised form
11 February 2011
Accepted 13 February 2011

Keywords:
Near-road
Barriers
Traffic
Air pollution
CFD
Modeling

ABSTRACT

Roadside noise barriers are common features along major highways in urban regions and are anticipated to have important effects on near-road air pollution through altering the dispersion of traffic emissions and resulting downstream concentrations. A 3-dimensional computational fluid dynamics (CFD) 6-lane road model has been developed to simulate roadside barrier effects on near-road air quality and evaluate the influence of key variables, such as barrier height and wind direction. The CFD model matches an existing wind tunnel road model and comparison with the wind tunnel data guided the selection of the optimal turbulence model (Realizeable $k-\varepsilon$ turbulence model with a Schmidt number of 1.0). Under winds perpendicular to the road, CFD model simulations show that roadside barriers reduce the concentration of an inert gaseous tracer (χ), relative to a no-barrier situation, vertically up to approximately half the barrier height and at all horizontal distances from the road. At 20 m (3.3H, where $H = 6$ m) from the road, barriers of heights ranging from 0.5H to 3.0H reduce the maximum concentrations by 15–61% relative to a no-barrier case, with the location of the maximum shifted to occur near the top of the barrier. The near-road reduction comes at a penalty for on-road air pollutant concentrations: on-road pollution is projected to increase by a factor of 1.1–2.3 corresponding to barriers ranging from 0.5H to 3.0H. When the noise barrier is downwind of the road, a stagnant zone is formed behind the barrier and minor road emissions (e.g., 5% of the highway emissions strength) in this zone, such as a moderately traveled service road, have a magnified effect on concentrations immediately behind the barrier. Wind direction and barrier termination also play a critical role, with a spill-over of accumulated emissions upwind of the barrier strongly increasing near-road concentrations at one end of the barrier. These results imply that roadside barriers may mitigate near-road air pollution, although local meteorology, the barrier structure, and the degree of lee-side emission sources are critical factors determining the outcome.

Published by Elsevier Ltd.

1. Introduction

Elevated concentrations of air pollution adjacent to major roadways are a current public health concern. Field studies have quantified steep spatial concentration gradients of traffic-related pollutants (e.g., carbon monoxide, ultrafine particles, black carbon, oxides of nitrogen), with a maximum concentration occurring next to the road and dropping exponentially to background levels within several hundred meters of a major roadway (Zhu et al., 2002; Baldauf et al., 2008a; Beckerman et al., 2008; Hagler et al., 2009). Traffic emissions are linked to an exposure region of up to 300–500 m from the road and currently available health effects data are considered to be sufficient to associate traffic emissions with the exacerbation of asthma and to suggest a link with the onset of childhood asthma, non-asthma respiratory symptoms, impaired lung function, total mortality, and cardiovascular mortality (HEI, 2010 and references therein).

Several wind tunnel, numerical model, and field studies have indicated that roadside obstructions to air flow, such as tree stands or noise barriers, may have significant effects on vehicular emissions dispersion and ambient air pollutant concentrations (Bowker et al., 2007; Baldauf et al., 2008b; Heist et al., 2009; Wang and Zhang, 2009; Finn et al., 2010; Ning et al., 2010). Field measurements at a near-road site in Raleigh, North Carolina, revealed reductions in both carbon monoxide and ultrafine particles downwind of a 6 m high brick noise barrier along a busy roadway

* Corresponding author.
E-mail address: hagler.gayle@epa.gov (G.S.W. Hagler).

1352-2310/$ – see front matter Published by Elsevier Ltd.
doi:10.1016/j.atmosenv.2011.02.030

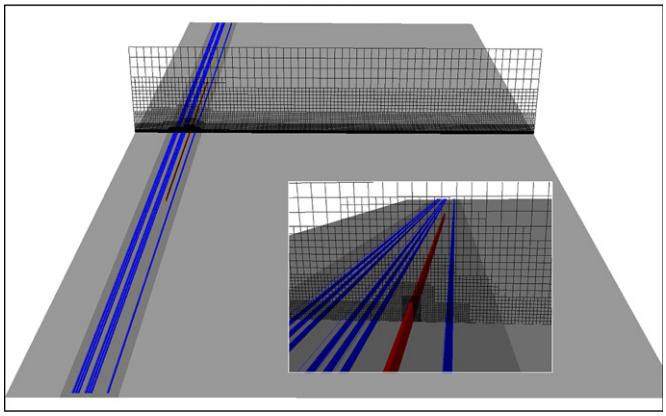

Fig. 1. CFD roadway model, showing the computational mesh with cell size ranging 0.25–8 m.

(Baldauf et al., 2008b). A similar study in California determined lower pollution levels in the lee of a barrier, relative to a clearing, but that concentrations rose to levels above the clearing further downwind (Ning et al., 2010). In addition, a field experiment studying the dispersion of a SF6 line source upwind of a 6 m high straw bale barrier, constructed to simulate a solid noise barrier, found concentration reductions downwind of the barrier relative to concentrations from the same source in a clearing, for a range of meteorological stability categories (Finn et al., 2010). Wind tunnel experiments also show that for crosswind conditions, a roadside barrier leads to a vertical lofting of the roadway emissions and decrease of ground-level concentrations in the wake of a barrier, relative to a no-barrier case (Heist et al., 2009).

Table 1
Traffic emissions dispersion modeling scenarios.

Case	Barrier height ($H = 6$ m)	Wind speed[a]	Wind direction	Service road
A	0.5*H*	4 m s^{-1}	90°	0
B	*H*	4 m s^{-1}	90°	0
C	1.5*H*	4 m s^{-1}	90°	0
D	3*H*	4 m s^{-1}	90°	0
E	*H*	4 m s^{-1}	75°	0
F	*H*	4 m s^{-1}	45°	0
G	*H*	4 m s^{-1}	90°	5%
H	*H*	4 m s^{-1}	90°	10%

[a] Wind speed at height of 20*H*.

The use of roadside barriers to mitigate near-road air quality is an attractive concept, given significant challenges associated with other means of reducing near-road air pollution in a timely manner. In densely populated areas with major roadways already in existence, options for reducing near-road exposure to populations include traffic management, emissions controls, or relocation of exposed populations. Current emissions controls in the United States are projected to significantly improve air quality; however, the improvements will be gradual as older and higher-emitting

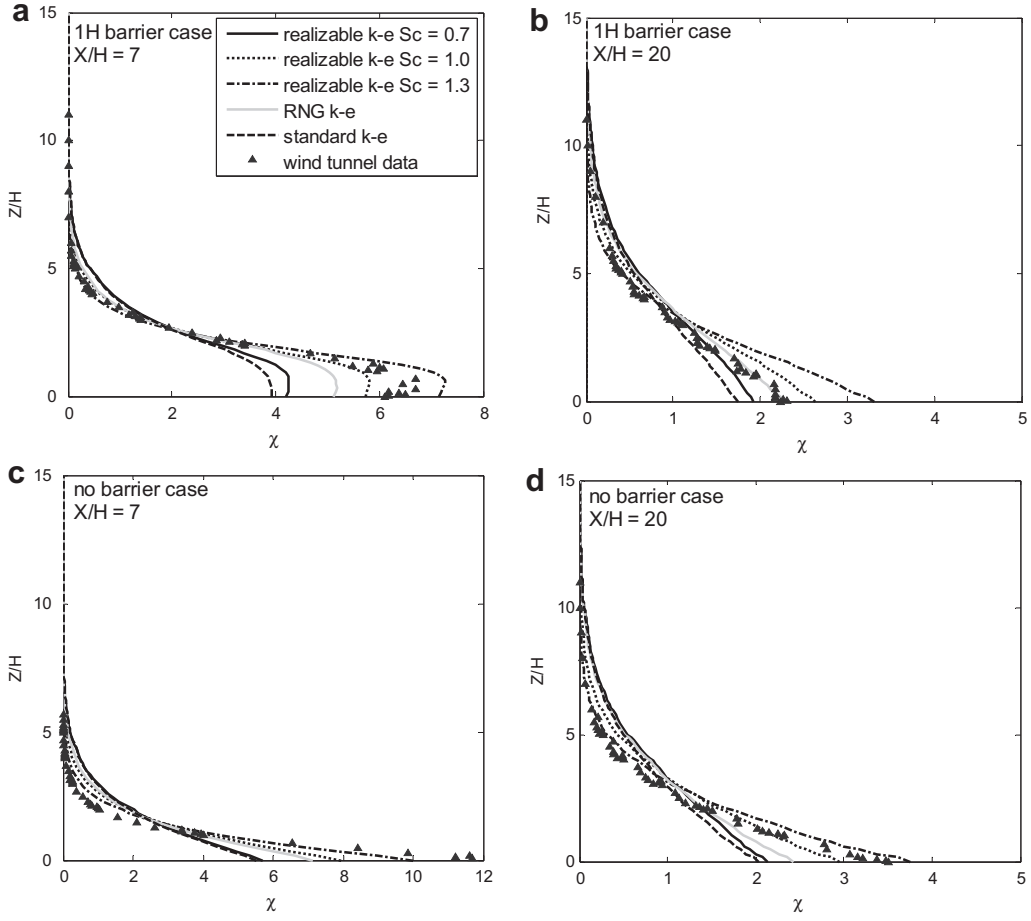

Fig. 2. Comparison of wind tunnel with various CFD vertical concentration profiles at different downwind distances of a road results for a barrier of 1*H* at $X/H = 7$ (a) and $X/H = 20$ (b); and for a no-barrier case at $X/H = 7$ (c), and $X/H = 20$ (d). The center of the road is located at $X/H = 0$, the edge of the road is at 2.35*H*, and the barrier position is at 3*H* (3.9 m from the road edge).

vehicles are retired from the fleet. Roadside barriers, on the other hand, can be a more immediate tool to improve near-road air quality, if demonstrated to provide this positive effect.

In order to further understand the conditions that favor or disfavor air quality improvement by roadside barriers, a computational fluid dynamics (CFD) roadside barrier model was developed. This barrier model was designed to mimic a wind tunnel experiment design by Heist et al. (2009) and evaluated against the wind tunnel results. The CFD model was then varied to observe the effect of changing the roadside barrier height and wind direction, and the addition of a minor service road as an emissions source downwind of the barrier.

2. Methods

2.1. Model geometry

A 3-dimensional CFD simulation of a generic highway was designed using commercial CFD code, FLUENT (ANSYS, Inc.). This modeled scenario matches an existing wind tunnel model (Heist et al., 2009), in terms of road configuration and atmospheric boundary layer properties. The CFD modeled scenario consists of a six-lane divided highway which serves as a source of turbulence and emissions of an inert gaseous tracer with the same density as air. A solid 6 m (1*H*) high and 0.5 m thick wall is located along one side of the highway. For the wind tunnel matching simulation, the wall was continuous throughout the domain and located 3.9 m from the nearest lane of traffic. In the CFD simulations that followed, the wall dimensions more closely matched a site in Raleigh, NC where field data have been collected (Baldauf et al., 2008a,b) – a 6 m high, 0.5 m thick wall that is located at 5 m from the nearest lane of traffic, and having a discrete length. In the model, the wall spans 750 m of the roadway, with no obstructions to flow for a stretch of the roadway before and after (Fig. 1). This design allows changes in the pollutant dispersion due to the barrier to be directly assessed relative to the clearing and also allows the effect of the barrier edges to be observed. Downwind of the barrier, a single lane service road is added for certain scenarios to test the effect of a minor emissions source in the wake of a barrier. When active, the emissions strength of this service road is set at 5 or 10% relative to the highway emissions (e.g., 7500–15,000 Annual Average Daily Traffic [AADT] vs. 150,000 AADT). The single lane service road is positioned at 20 m (3.33*H*) from the nearest highway traffic lane.

The model is oriented with the solid barrier on the downwind side of the roadway, with the model domain extending 800 m downwind of the roadway (Fig. 1). In near-road field studies, air pollution impact from major roadways is commonly detected at distances of several hundred meters, although under unique meteorological conditions the spatial extent of near-road air pollution can be up to several kilometers (Hu et al., 2009). This model domain is designed to focus on impacts within several hundred meters of a road. For scenarios with perpendicular winds, the model domain is 2000 m along the road axis, 900 m perpendicular to the road, and 200 m in height. The model has a graduated mesh, ranging from 0.25 m in close proximity to the barrier

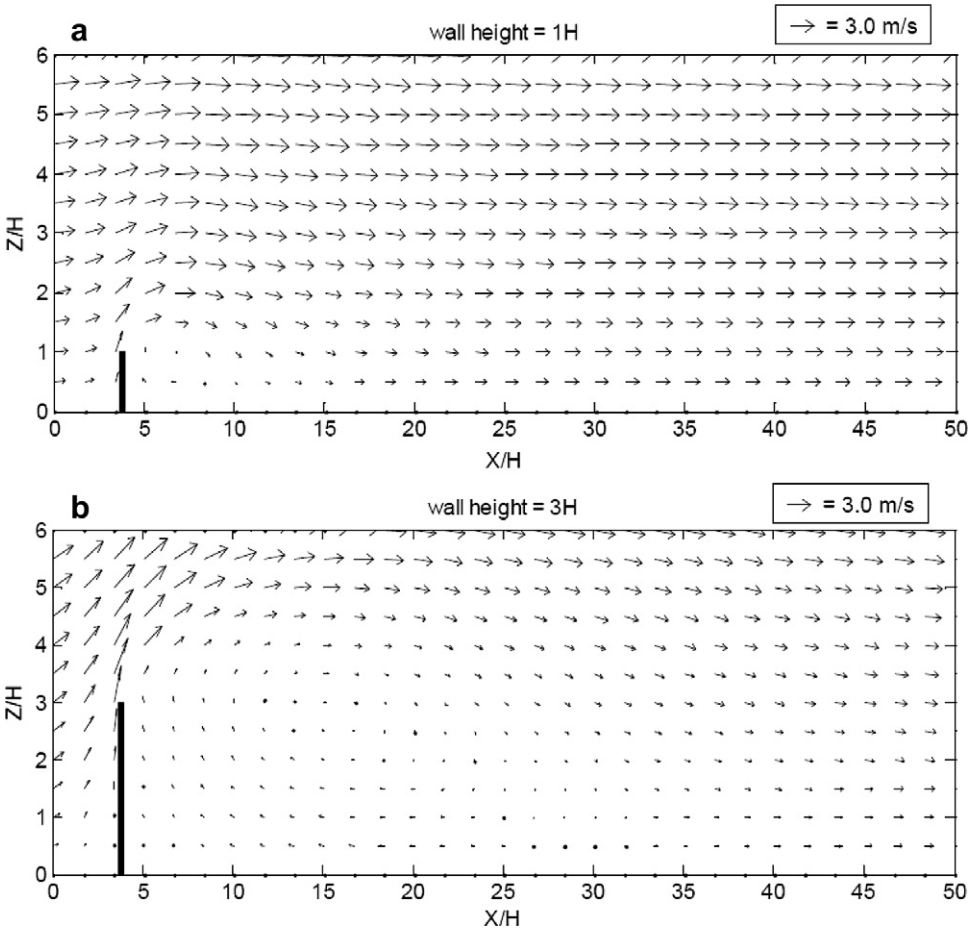

Fig. 3. Wind vectors in presence of a barrier of 6 m (a) and 18 m (b) height.

and increasing with distance from the road/barrier to 8 m maximum. The mesh was constructed using the commercial software Harpoon, which produces a body-fitted, hex-dominant mesh based upon an octree decomposition of the domain. The optimal mesh configuration was found by starting with a coarse mesh and then using successively finer meshes while observing the effect of the mesh size on the CFD solution. The process was continued until further refinements did not significantly alter the solution.

Ultimately, four different mesh configurations (trial meshes) were tested. Each of the trial meshes was characterized by a "base" size, which is the length of the side of the largest cell in the domain. The base sizes of the trial meshes were 16, 12, 8, and 6 m, while the corresponding smallest cell sizes (five levels down in the octree) were 0.5, 0.375, 0.25, and 0.1875 m respectively. A steady-state flow was simulated perpendicular to the barrier, and vertical profiles of velocity were monitored 10 m upstream of the barrier and at 10, 50, and 100 m downstream of the barrier. In addition, the along-flow velocity was monitored at the barrier height both upstream and downstream of the barrier. The coarsest mesh (base = 16 m) failed to resolve the flow gradients near the barrier, which is not unexpected since the mesh size near the barrier for that case was equal to the barrier width. The remaining cases did a better job of capturing the gradients near the barrier, and converged to a similar solution at all profile locations. The base = 6 m case did not significantly affect the solution compared to the base = 8 m case; therefore the base = 8 m case was chosen as the mesh configuration for the remainder of the study since it requires less computer memory. The overall mesh size ranges from 25.7 to 29.7 million cells and the model simulations demands 1300–2800 CPU hours to complete.

The first phase of model development focused on the selection of an appropriate turbulence model to best-fit the wind tunnel results. Details of this evaluation and selection are presented below. After satisfactory evaluation of the CFD model with wind tunnel experimental results, this base model is then used to perform the second phase of research – constructing multiple model scenarios (Table 1) changing barrier height, wind direction, and access road emissions strength, and observing the impact on traffic-related emissions dispersion and resulting near-road air quality. Model data outputs were analyzed and plots were generated using MATLAB (version R2009b) data analysis software.

2.2. Turbulence model selection based on comparison with wind tunnel data

The CFD base road model is designed to match a wind tunnel model that has been previously described (Heist et al., 2009). In short, the wind tunnel model is at a 1:150 scale and includes a six-lane, divided roadway. Upwind of the roadway, a boundary layer representative of an urban environment is developed using Irwin spires (Irwin, 1981), followed by a series of roughness tabs. The roughness tabs (3.8 cm high and 7.6 cm wide) cover the upwind fetch of the wind tunnel from 11 m upwind of the model roadway to 55 cm upwind. The wind tunnel floor is smooth in the vicinity of the roadway and the roughness tabs resume 165 cm downwind of the roadway. The resulting boundary layer at the model has a roughness length of 0.27 cm (0.36 m equivalent full-scale) and a friction velocity of 0.25 m s^{-1}. The wind speed at the top of the boundary layer (165 cm) is maintained at 4.7 m s^{-1}. The Reynolds number based on barrier height (4 cm) is 12,500. Wind velocities are measured using Laser Doppler Velocimetry (LDV), measuring the transport of smoke generated upwind of the spires. Tracer gas (ethane) is released along a section of the roadway, with an array of surface-level holes simulating six continuous line sources along the roadway. Small blocks (0.6 cm × 0.6 cm × 1.2 cm tall) are positioned 0.1 cm upwind of each emission hole to distribute the emissions vertically over the height of an average sized automobile. Concentrations downwind of the roadway are measured using Rosemount Model 400A hydrocarbon analyzers. To compute the velocity and concentration results, signals were sampled at 20 Hz over 120 s intervals. Results of the wind tunnel data, as well as the computational fluid dynamics model, are presented in normalized concentration units ($\chi = CU_rL_xL_y/Q$), where C is the background-adjusted concentration, U_r is the reference wind speed measured at a full-scale equivalent of 30 m, Q is the tracer gas emissions rate, and L_x and L_y are the dimensions of the source section. The wind tunnel concentration data is processed, as documented in Heist et al. (2009), to simulate the effect of an infinitely long roadway source.

The inlet boundary of the CFD model was defined as a velocity inlet. Inlet profiles for mean velocity, TKE, and ε were derived via a 2D case with periodic boundary condition that simulates a fully developed atmospheric boundary layer with a logarithmic profile, matching the mean velocity and TKE of the approach flow in the wind tunnel. A pressure outlet was specified at the downstream end of the domain. Symmetry conditions were imposed on the sides and top of the domain. The ground was set as wall condition with roughness $z_0 = 0.05$ m, which simulates the relatively smooth floor of the wind tunnel testing area without roughness tabs.

For all simulations, the FLUENT code solves Reynolds-averaged Navier–Stokes (RANS) equations with the gradient diffusion assumption for the turbulent scalar fluxes in the transport equation

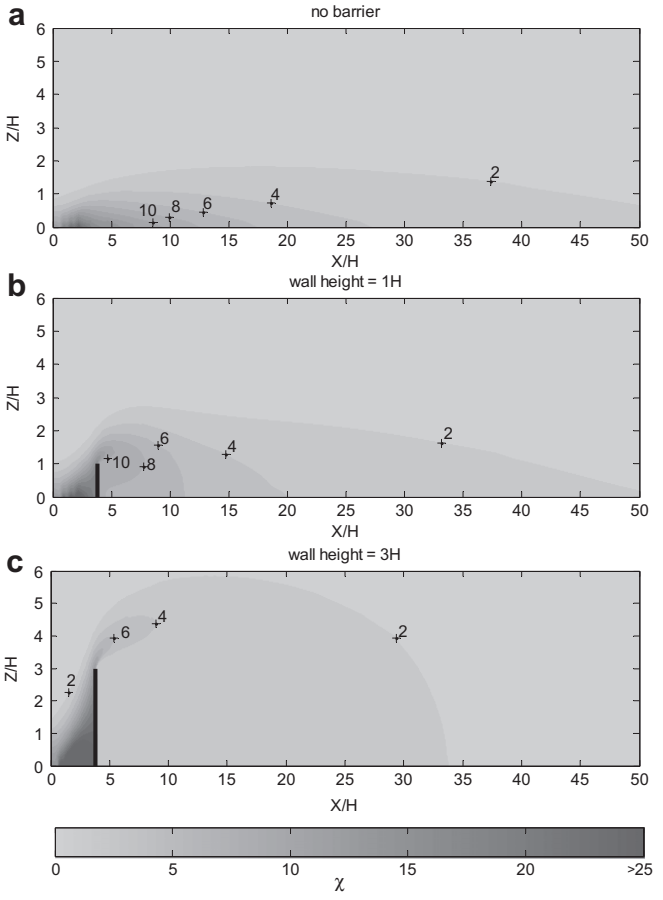

Fig. 4. χ for scenarios with orthogonal winds and cases with no barrier (a), barrier of height H (b), and barrier of height $3H$ (c).

for the passive scalar, which was used to model the concentrations. Second-order discretization schemes were chosen to increase accuracy and reduce numerical diffusion. Standard discretization was used for the pressure terms and second-order upwind for all other variables. For pressure–velocity coupling, the SIMPLE (Semi-Implicit Method for Pressure Linked Equations) algorithm was used to improve convergence.

The k–ε turbulence model with standard wall functions and its variations available in the FLUENT code are examined in this study. First proposed by Launder and Spalding (1972), the k–ε model has been applied to a wide range of practical engineering flows thanks to its robustness, economy, and reasonable accuracy. It has been increasingly adapted to the study of the atmospheric boundary layer (Detering and Etling, 1985; Richards and Hoxey, 1993; Alinot and Masson, 2005). Here, three variations of the k-ε turbulence model are applied to observe the agreement between the CFD road model and wind tunnel model data – Standard k–ε, Re-Normalization Group (RNG) k–ε, and Realizable k–ε. All three models have similar forms, but differ in the method of calculating turbulent viscosity, the turbulent Prandtl numbers, the generation and destruction terms in the ε equation (ANSYS, 2009). In addition, to simulate species transport in turbulence flows, an important model parameter is the turbulent Schmidt number (Sc_t), which is the ratio of the turbulent transfer of momentum (turbulent viscosity) to turbulent transfer of mass (turbulent diffusivity). The role of Sc_t in dispersion modeling has not been studied extensively, especially within urban areas. Sc_t values ranging from 0.18 to 1.34 have been reported based on observations over open field under different atmospheric stability and wind conditions (Flesch et al., 2002). In a neutrally stratified wind tunnel flow, Koeltzsch (2000) has shown Sc_t to be a function of height, although common practice in CFD modeling is to use a constant Sc_t within the boundary layer. In FLUENT code, the default Sc_t value is 0.7. Previous work (Tang et al., 2006) on CFD modeling of atmospheric dispersion over open fields has shown simulations using Sc_t of 1.0 performed best when compared with field measurements. Here, for the CFD to wind tunnel comparisons, values selected for Sc_t were 0.7, 1.0, and 1.3.

3. Results and discussion

3.1. Evaluation of CFD model with wind tunnel experimental data

The standard, RNG, and three variations of Realizable k–ε turbulence models produce generally similar vertical concentration distributions for the 1H (6 m) barrier (Fig. 2a,b) and no-barrier (Fig. 2c,d) cases, in comparison to the wind tunnel. While comparisons of turbulent kinetic energy and vertical velocity values are also assessed (Figs. S1 and S2 in Supplementary Information), the stronger emphasis for agreement is on the simulated pollutant concentrations in order to draw conclusions on barrier effects for near-road air pollution. In close proximity to the road (7H, road center at 0H), behind-barrier vertical concentration gradients as measured by the wind tunnel are reasonably matched by the Realizable model simulations with $Sc_t = 1.0$ and $Sc_t = 1.3$. With $Sc_t = 1.0$, the simulation slightly underpredicts ground-level concentrations in both cases and with $Sc_t = 1.3$ it overpredicts for

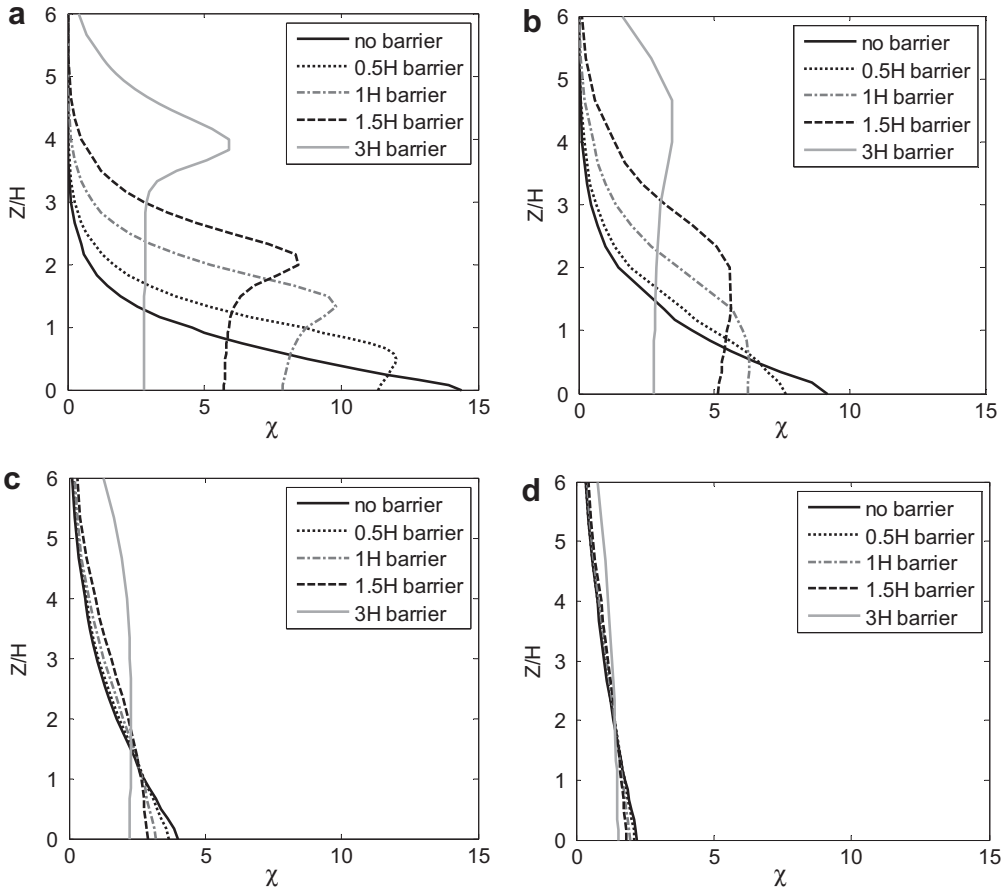

Fig. 5. Vertical distribution of normalized concentrations (χ) at 20 m/3.3H (a), 50 m/8.3H (b), 150 m/25H (c), and 300 m/50H (d) from the edge of the roadway under perpendicular winds, for barriers of 3–18 m compared with a no-barrier scenario. The barrier is located 9.5 m from the road edge.

the behind-barrier comparison and is in agreement for the no-barrier comparison. The standard, RNG, and Realizable with $Sc_t = 0.7$ k–ε models all significantly underpredict ground-level concentrations, although all models agree well above a height of approximately 3H.

At a greater distance from the roadway (20H), the RNG and Realizable with $Sc_t = 1.0$ are in closest agreement with wind tunnel results for the 1H barrier case (Fig. 2c), while Realizable with $Sc_t = 1.3$, followed by Realizable with $Sc_t = 1.0$, is in closest agreement for the no-barrier case (Fig. 2d). While no turbulence model produces ideal agreement between the wind tunnel and CFD model results, Realizable with $Sc_t = 1.0$ provides the most consistent agreement for both the 1H barrier and no-barrier models. Thus, the expanded CFD roadway model scenarios utilize the Realizable model with $Sc_t = 1.0$ for all simulations.

3.2. Barrier height effect

After completing the selection of the Realizable turbulence model ($Sc_t = 1.0$), a series of CFD model scenarios (A–D in Table 1) were then constructed to evaluate the influence of barrier height on air pollutant concentrations. Barrier heights ranging 0.5H to 3H (3–18 m) are modeled to encompass the range of noise barrier or vegetation heights in existence alongside roadways, although it should be noted that all scenarios to be discussed involve solid, not porous, barriers. With winds perpendicular to the roadway, the presence of a barrier leads to a vertical lofting of emissions (Fig. 3a,b), with an increasing vertical velocity component on the roadway side of the wall with increasing barrier height. Downwind of the barrier, a recirculation zone forms when winds are from the roadway. This mixing zone extends vertically up to or slightly exceeding the barrier height and horizontally by approximately a factor of 10 times the barrier height – approximately 10H (60 m) for the 1H barrier and 30H (180 m) for the 3H barrier. The gradient in velocity at the barrier edge and downwind of the barrier generates turbulent kinetic energy that increases with barrier height (Fig. S3 in Supplementary Information).

The vertical lofting of on-road emissions leads to reduced concentrations at the ground level, relative to the no-barrier case as shown in concentration contours of an X–Z slice of the CFD model (Fig. 4). For example, the horizontal extent of $\chi = 4$ contour downwind of the road reaches to approximately 25H (150 m) for the no-barrier case, but to 20H (120 m) for the 1H barrier case, a 20% reduction in the extent of impact. For a very tall barrier (3H), the concentrations are substantially reduced behind the barrier, with $\chi = 4$ only occurring near the top of the barrier. This barrier-effected reduction of near-road air pollution generally agrees with past findings determining lower concentrations behind barriers, relative to a clearing, when downwind of a highway (Bowker et al., 2007; Baldauf et al., 2008b; Heist et al., 2009; Finn et al., 2010). However, some studies suggest that roadside barriers may lead to higher pollutant levels relative to a clearing at greater distances from the road (>80 m) where the vertically lofted traffic emissions plume reattaches (Bowker et al., 2007; Ning et al., 2010), which contrasts to the CFD model results.

Vertical concentration profiles (Fig. 5) for different barrier heights and a no-barrier scenario, at different distances from the roadway, reveal that a roadside barrier changes the vertical location of maximum concentration downwind of a road. At 20 m from the roadway (Fig. 5a), where high impact from the road is evident for a no-barrier concentration, ground-level concentrations are substantially lower behind barriers but are elevated with respect to a no-barrier scenario at heights exceeding roughly half of the barrier height. However, for all barrier cases, the maximum concentration over the entire vertical distance is reduced by 15–61%, with higher barriers associated with greater reductions in simulated air pollution. Ground-level concentrations are predicted to be lower, and upper-level concentrations higher, behind barriers relative to a clearing at distances up to 300 m or 50H from the road (Fig. 5b–d). However, the barrier effect and absolute concentrations taper with increasing distance, and only slight differences in the vertical concentration profile are discernible at 50H from the road.

The CFD model findings on the horizontal extent of barrier impact agree with a tracer field study that quantified reductions up to and potentially exceeding 30H or 180 m, the spatial limit of the field measurements (Finn et al., 2010). In a more complex near-road environment in Raleigh, North Carolina, *in situ* measurements of ultrafine particles found decreases in concentrations behind a solid barrier, relative to a clearing, up to 50–100 m in distance from a major roadway, depending on the particle size (Baldauf et al., 2008b). A modeling study, using the Quick Urban Industrial Complex (QUIC) empirical dispersion model, of the same Raleigh field site suggests that when buildings and trees are located behind the barrier, additional mixing occurs and causes significant spatial variability in the near-road air pollution (Bowker et al., 2007). A recent study in California observed reduced concentrations of several pollutants immediately behind a barrier, when downwind of the road, but measured a localized increase in concentrations at distances further downwind (80–100 m) (Ning et al., 2010). While the CFD model presented in this study predicts reductions in concentrations behind the barrier at distances exceeding 100 m, it

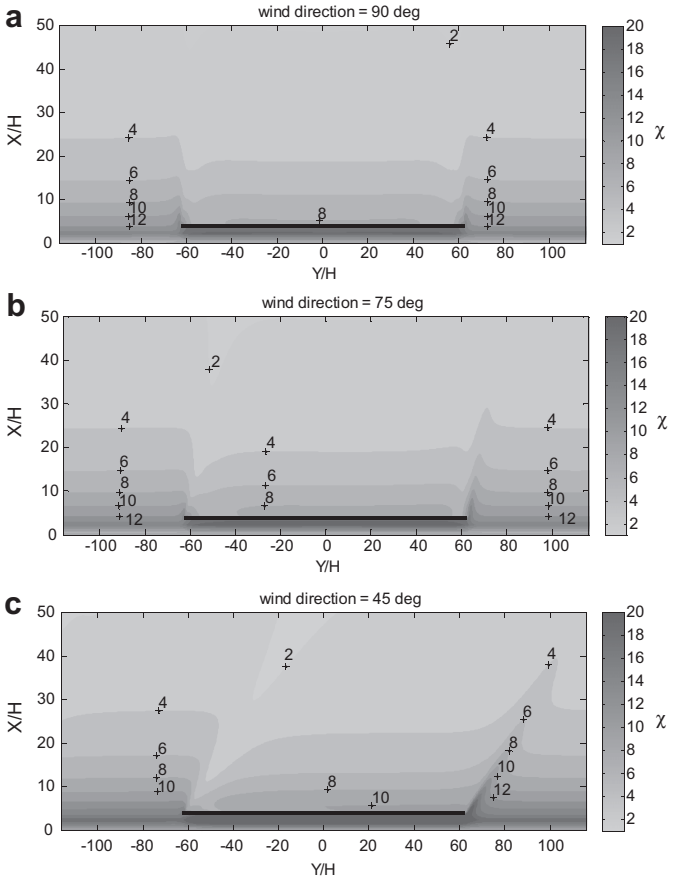

Fig. 6. Top view of modeled air pollutant concentrations (χ) at 2 m above the ground surface, for cases with a barrier of height H and incident wind directions of 90 deg (a), 75 deg (b), and 45 deg (c). The barrier is located between −62.5 and +62.5 Y/H (750 m in length).

is uncertain whether the barrier-effect would be detectable in more true-to-life field or modeling scenarios with other factors, such as homes or distributed trees, altering air flow patterns. In addition, the model does not currently cover the more complex emitted species which are not inert in the atmosphere, such as particulates which can undergo coagulation and condensational growth after emission (Zhang et al., 2004) as well as potential enhanced removal from the atmosphere by deposition to barrier surfaces.

While ground-level concentrations are reduced behind the barrier, relative to an unobstructed flow situation, on-road concentrations appear to increase with a barrier present (Fig. 4). For barrier heights ranging 0.5*H* to 3*H*, on-road concentrations increase correspondingly by a factor of 1.1–2.3, relative to a no-barrier situation. This finding has implications for in-traffic exposure by passengers in vehicles and for bicyclists or pedestrians that may be located on the road side of the barrier.

3.3. Impact of changing wind direction

While the majority of current field and wind tunnel results regarding barrier effects on near road air quality focus on winds perpendicular to the road, this model extends the analysis to evaluate the effect of oblique wind directions (scenarios B, E, and F in Table 1). In particular, it is of interest to understand the effect of barrier endpoints with changing wind direction. A top view of the model (Fig. 6a–c) shows ground-level (2 m) concentration contours under wind directions varying from perpendicular (90 deg) to increasing oblique angles (75 and 45 deg). Under perpendicular winds, it is seen that a slightly higher concentration zone exists at both edges of the barrier, due to a spill-over of accumulated traffic emissions on the road side of the barrier. This spill-over effect was apparent in recent field measurements conducted in Raleigh, NC, which noted that pollutant concentrations downwind of a roadside barrier were not substantially lower than that in a clearing until over approximately 40 m from the edge of the barrier (Baldauf et al., 2008b).

Under oblique winds, it is seen that the region of highest near-road concentrations shifts to the far edge of the barrier, while a reduced concentration zone appears downwind of the other end of the barrier. In addition to this barrier edge effect under oblique winds, the oblique wind direction also affects the on-road concentrations, with the road-parallel component of the wind accumulating concentrations along the road. Under slight wind angles, this effect is minor. However, as the wind angles move closer to parallel (<45 deg), the on-road accumulation leads to a blurring of clearing versus barrier-effected zones and requires additional model development to study.

3.4. Effect of minor road source behind barrier

Another level of complexity was introduced by adding a second traffic emissions and turbulence source, representative of a service

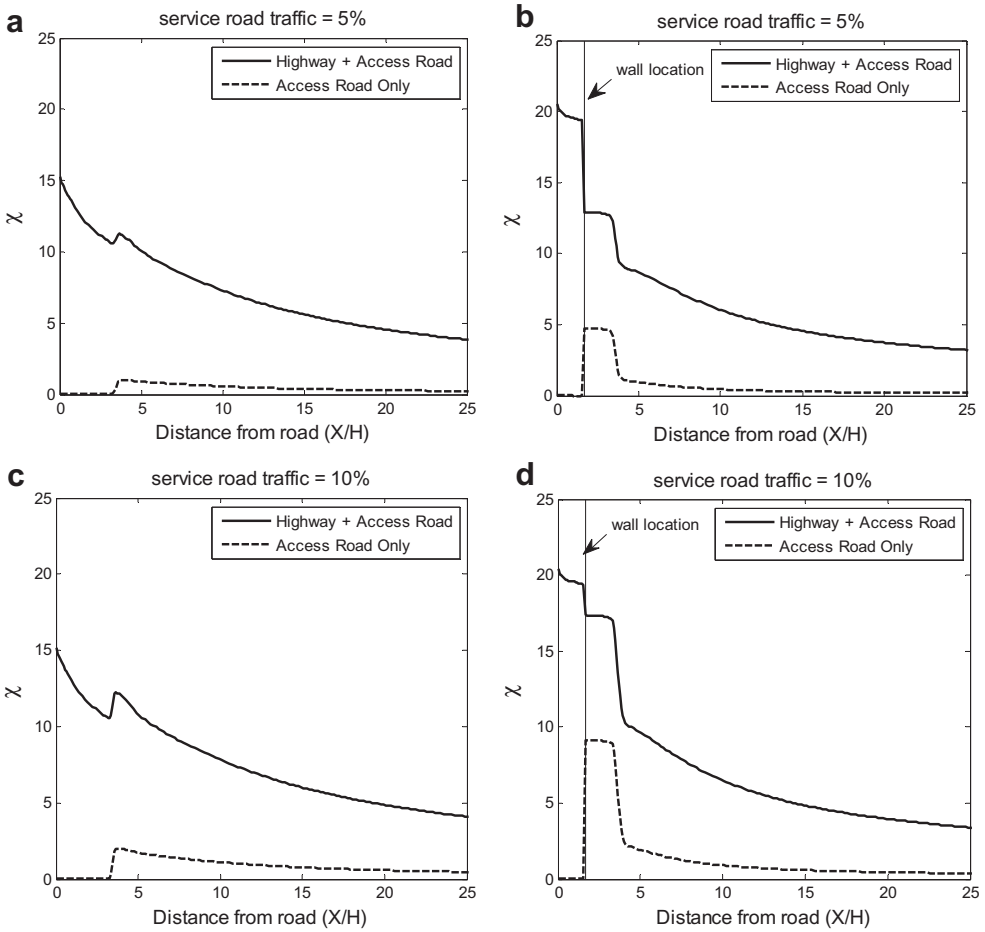

Fig. 7. Modeled total χ and access road-attributed χ at 1/3*H* (2 m) above ground as a function of distance from the road up to 25*H* (150 m). The access road is located parallel to the highway, with traffic levels at 5% (a, b) and 10% (c, d) of the highway traffic volume. Two scenarios are shown – a no barrier case (a, c) and a case with a barrier of height *H* (6 m) located between the highway and service road (b, d). This figure has the road edge set to 0H and the wall positioned at 1.6*H*.

road or neighborhood street, located downwind of the barrier (scenarios G and H in Table 1). Field data are sparse on the effect of secondary roads coupled with obstructions to air flow from the road, but the limited data show that this factor merits further investigation. A recent mobile monitoring near-road study measured higher levels of CO, but not UFPs, along transects with a highway frontage road behind a 5-m solid barrier, relative to a transect with a frontage road but no barrier, which they explained as a combined effect of differing vehicle emissions on the highway versus frontage road and modification of emissions dispersion by the barrier (Hagler et al., 2010).

For the CFD model scenario with winds perpendicular to the road and with a 1*H* barrier, the small amount of emissions (5% or 10% of the highway emissions strength) is shown to have a significant effect for approximately 2*H* (12 m) behind the wall, constituting 40–50% of the total concentration immediately behind the wall and exceeding the total concentration observed for the no-barrier situation. In comparison, the maximum contribution of the service road to near-road air pollution with no barrier present is approximately 10%. Past this zone, the contribution of the service road to near-road concentrations tapers rapidly and contributes less than 10–20% to downwind concentrations, with total concentration behind the barrier reduced to less than the no-barrier case past the 2*H* zone (Fig. 7a–d). This result indicates that even minor roads located behind barriers, can have a magnified impact when emitting in the recirculation zone that is created behind barriers when downwind of a road.

4. Conclusions

Roadside barriers, including structural noise barriers and vegetative buffers, are useful in the reduction of noise and aesthetic impacts from major traffic corridors in urban regions. This study evaluates whether solid noise barriers may also provide mitigation for traffic-related air pollution that occurs up to several hundred meters from a major roadway and is associated with adverse health effects (HEI, 2010). If roadside structural and/or vegetative barriers are shown to improve air quality, the added air quality benefit may justify the addition of barriers to existing roadside developments or the preservation of existing roadside barriers.

This study utilizes computational fluid dynamics modeling to simulate the transport of inert gaseous emissions from a 6-lane roadway and resulting pollution of the near-road environment, with and without roadside barriers present. The results suggest that solid barriers, which may also loosely represent low-porosity vegetation, do significantly reduce maximum and ground-level concentrations downwind of a major roadway relative to an unobstructed flow situation. The presence of a roadside barrier induces a vertical lofting of the on-road emissions, mixing the emissions with clean air above the road and reducing the overall concentration in the plume. The vertical lofting of the emissions changes the location of the maximum concentration to occur near the top of the barrier. The reduction in air flow by barriers increases on-road concentrations on the upwind side of the barrier, which worsen with increasing barrier height. The presence of a roadside barrier also leads to a mixing zone located in the wake of the barrier, where a small degree of emissions (e.g., 5–10% of the highway strength) can significantly increase concentrations immediately behind the barrier. These results also suggest that on-road concentrations are likely higher when the barrier is upwind of the highway, which has been illustrated in wind tunnel results presented by Heist et al. (2009).

This study agrees with and builds upon past work addressing road configurations and roadside features (Bowker et al., 2007; Baldauf et al., 2008b; Heist et al., 2009; Wang and Zhang, 2009; Finn et al., 2010; Ning et al., 2010), suggesting that the design of roads and roadside structures, along with local meteorology, are important factors determining near-road air pollution levels. This study shows that the vertical profile of near-road traffic-related pollutant concentrations is dramatically altered by barriers, which has implications for estimating human exposure, air monitoring data interpretation, and may inform future site design. Other critical considerations are local meteorology, the location of other emission sources in the near-road environment, and additional road or roadside design elements that may also modify air flow.

5. Disclaimer

This document has been reviewed in accordance with U.S. Environmental Protection Agency policy and approved for publication. Mention of trade names or commercial products does not constitute endorsement or recommendation for use. The views expressed in this journal article are those of the authors and do not necessarily reflect the views or policies of the U.S. Environmental Protection Agency.

Acknowledgements

This research was funded by the U.S. EPA Office of Research and Development. This research would not be possible without the support of Joe Retzer and Heidi Paulsen with EPA's Environmental Modeling and Visualization Center. We also would like to thank Mike Uhl from Lockheed Martin's Information Systems & Global Services group. Computational resources were managed by EPA's High Performance Computing center. Authors would also like to thank several members of EPA's near-road team contributing to research related to mitigation of near-road impact by barriers, including Richard Baldauf, Vlad Isakov, Laura Jackson, Dan Costa, Carlos Nunez, Richard Shores, Sue Kimbrough, Eben Thoma, and Jim Hirtz.

Appendix. Supplementary data

Supplementary data associated with this article can be found in the online version, at doi:10.1016/j.atmosenv.2011.02.030.

References

Alinot, C., Masson, C., 2005. κ-ε model for the atmospheric boundary layer under various thermal stratifications. Journal of Solar Energy Engineering-Transactions of the ASME 127, 438–443.

ANSYS, Inc., 2009. FLUENT 12.0 User's Guide.

Baldauf, R., Thoma, E., Isakov, V., Long, T., Weinstein, J., Gilmour, I., Cho, S., Khlystov, A., Chen, F., Kinsey, J., Hays, M., Seila, R., Snow, R., Shores, R., Olson, D., Gullett, B., Kimbrough, S., Watkins, N., Rowley, P., Bang, J., Costa, D., 2008a. Traffic and meteorological impacts on near road air quality: summary of methods and trends from the Raleigh Near Road Study. Journal of the Air & Waste Management Association 58, 865–878.

Baldauf, R., Thoma, E., Khlystov, A., Isakov, V., Bowker, G., Long, T., Snow, R., 2008b. Impacts of noise barriers on near-road air quality. Atmospheric Environment 42, 7502–7507.

Beckerman, B., Jerrett, M., Brook, J.R., Verma, D.K., Arain, M.A., Finkelstein, M.M., 2008. Correlation of nitrogen dioxide with other traffic pollutants near a major expressway. Atmospheric Environment 42, 275–290.

Bowker, G.E., Baldauf, R., Isakov, V., Khlystov, A., Petersen, W., 2007. The effects of roadside structures on the transport and dispersion of ultrafine particles from highways. Atmospheric Environment 41, 8128–8139.

Detering, H.W., Etling, D., 1985. Application of the E–ε turbulence model to the atmospheric boundary layer. Boundary-Layer Meteorology 33, 113–133.

Finn, D., Clawson, K.L., Carter, R.G., Rich, J.D., Eckman, R.M., Perry, S.G., Isakov, V., Heist, D.K., 2010. Tracer studies to characterize the effects of roadside noise barriers on near-road pollutant dispersion under varying atmospheric stability conditions. Atmospheric Environment 44, 204–214.

Flesch, T.K., Prueger, J.H., Hatfield, J.L., 2002. Turbulent Schmidt number from a tracer experiment. Agricultural and Forest Meteorology 111, 299–307.

Hagler, G.S.W., Baldauf, R.W., Thoma, E.D., Long, T.R., Snow, R.F., Kinsey, J.S., Oudejans, L., Gullett, B.K., 2009. Ultrafine particles near a major roadway in

Raleigh, North Carolina: downwind attenuation and correlation with traffic-related pollutants. Atmospheric Environment 43, 1229–1234.
Hagler, G.S.W., Thoma, E.D., Baldauf, R.W., 2010. High-resolution mobile monitoring of carbon monoxide and ultrafine particle concentrations in a near-road environment. Journal of the Air & Waste Management Association 60, 328–336.
HEI Panel on the Health Effects of Traffic-Related Air Pollution, 2010. Traffic-Related Air Pollution: A Critical Review of the Literature on Emissions, Exposure, and Health Effects. Health Effects Institute, Boston, Mass.
Heist, D.K., Perry, S.G., Brixey, L.A., 2009. A wind tunnel study of the effect of roadway configurations on the dispersion of traffic-related pollution. Atmospheric Environment 43, 5101–5111.
Hu, S.S., Fruin, S., Kozawa, K., Mara, S., Paulson, S.E., Winer, A.M., 2009. A wide area of air pollutant impact downwind of a freeway during pre-sunrise hours. Atmospheric Environment 43, 2541–2549.
Irwin, H., 1981. The design of spires for wind simulation. Journal of Wind Engineering and Industrial Aerodynamics 7, 361–366.
Koeltzsch, K., 2000. The height dependence of the turbulent Schmidt number within the boundary layer. Atmospheric Environment 34, 1147–1151.
Launder, B.E., Spalding, D.B., 1972. Lectures in Mathematical Models of Turbulence. Academic Press, London, England.
Ning, Z., Hudda, N., Daher, N., Kam, W., Herner, J., Kozawa, K., Mara, S., Sioutas, C., 2010. Impact of roadside noise barriers on particle size distributions and pollutants concentrations near freeways. Atmospheric Environment 44, 3118–3127.
Richards, P.J., Hoxey, R.P., 1993. Appropriate boundary conditions for computational wind engineering using the κ–ε turbulence model. Journal of Wind Engineering and Industrial Aerodynamics 46 (7), 145–153.
Tang, W., Huber, A.H., Bell, B., Schwarz, W., 2006. Application of CFD simulations for short-range atmospheric dispersion over open fields and within arrays of buildings. In: AMS 14th Joint Conference on the Application of Air Pollution Meteorology with the A&WMA, Atlanta, Georgia. J1.8.
Wang, Y.J., Zhang, K.M., 2009. Modeling near-road air quality using a computational fluid dynamics model, CFD-VIT-RIT. Environmental Science & Technology 43, 7778–7783.
Zhang, K.M., Wexler, A.S., Zhu, Y.F., Hinds, W.C., Sioutas, C., 2004. Evolution of particle number distribution near roadways. Part II: the 'road-to-ambient' process. Atmospheric Environment 38, 6655–6665.
Zhu, Y.F., Hinds, W.C., Kim, S., Sioutas, C., 2002. Concentration and size distribution of ultrafine particles near a major highway. Journal of the Air & Waste Management Association 52, 1032–1042.